Engineering Structures 277 (2023) 115428

Contents lists available at ScienceDirect

Engineering Structures

journal homepage: www.elsevier.com/locate/engstruct

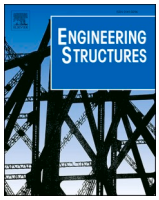

Analysis of failure mechanisms of adhesive joints modified by a novel additive manufacturing-assisted method

Armin Yousefi Kanani [a], Xing-Er Wang [b], Xiaonan Hou [b,*], Allan E.W. Rennie [b], Jianqiao Ye [b]

[a] Mechanical Engineering Group, School of Engineering, University of Kent, Canterbury CT2 7NL, United Kingdom
[b] Department of Engineering, Faculty of Science and Technology, Lancaster University, Lancaster LA1 4YW, United Kingdom

ARTICLE INFO

Keywords:
Multi-material joint
Adhesive joints
Discrete element method
Finite element method
Additive manufacturing

ABSTRACT

The research presented in this paper used an innovative method to modify the configuration of adhesively bonded joints for improved mechanical performance. Additive manufacturing was employed to produce sacrificial support structures with a water-soluble filament (Polyvinyl Alcohol). The design freedom offered by additive manufacturing makes it easy to tailor fixtures to any geometry, which can be used to accurately make the desired fillet shape at the end of the adhesive bond line. In addition to the experimental tests, the finite element method (FEM) was used to study the stress distribution along the bond line for four different modified bonded joints, whilst the discrete element method (DEM) was used to estimate the joint failure load and crack path in the adhesive bond line due to its strength in describing the initiation and progression of micro-cracks. The results show that the novel manufacturing method can produce an accurate fillet at the end of the bond line, regardless of the adhesive type. The mechanical performance of the joints with the modified features increased significantly. Furthermore, the failure load and crack path obtained from the DEM model is in close agreement with experimental and finite element (FE) results. Hence, the failure mechanism of the hybrid joints is then summarised.

1. Introduction

The most recent data shows that the transportation sector is the biggest worldwide contributor to greenhouse gas emissions (28 % in the UK in 2018) [1]. The European Aluminium Association predicts a decrease of around 5.4 gCO_2/km in greenhouse gas emissions can be accomplished by reducing weight by 100 kg in a conventional internal combustion engine (ICE) vehicle [2]. One of the most effective methods to achieve lightweighting is to use advanced lightweight materials instead of conventional materials. In practice, this necessarily results in the use and fabrication of multi-material structures for which proper joining techniques are critical for the high performance of the overall structures. Among commonly available joining technologies, adhesive joints attract the most attention due to their advantage of enabling the development of lightweight, cost-effective and highly integrated structures with a better uniform load distribution and improved damage tolerance while protecting surface aesthetics.

In recent decades, the increased use of dissimilar joints in transport structures, such as bonding composites to metals, has necessitated the development of a method to improve the efficiency of these joints. Several methods for improving the efficiency of adhesively bonded joints have been addressed in the review papers [3–5]. Geometrical modification of the bonded structure is viewed as one of the major methods for improving the efficiency of the bonded joint by attempting to change the shape of adherends or adhesives. The most popular methods are tapering, rounding and notching the adherend/adhesive [6,7], changing the adherends shape [8], and optimising the adherends/adhesive thickness and length [9]. All of these approaches aim to reduce the concentration of shear and peel stresses at the ends of the bond line, which significantly benefit dissimilar single-lap joints. Since the shear stress concentrations are higher near the free edges of the interface between the adhesive and lower stiffness adherend [10], this results in an asymmetric stress distribution due to different longitudinal deformations at the bond-line ends [11]. These stress concentrations at the bond-line ends are important since high stresses likely trigger a crack initiation in the adhesive bond-line.

The finite element method (FEM) has become the most extensively used approach for predicting failure load and damage progression in adhesive joints. Da Silva and Adams [12] studied various configurations of the dissimilar double lap joint to find solutions for peel stress failure of composite adherends. Since the composite material has a low transverse (through the thickness) tensile strength, the peel stress at the free end of

* Corresponding author.
E-mail address: x.hou2@lancaster.ac.uk (X. Hou).

https://doi.org/10.1016/j.engstruct.2022.115428
Received 25 April 2022; Received in revised form 17 November 2022; Accepted 4 December 2022
Available online 13 December 2022

the bond-line can cause failure in the composite adherend before the adhesive layer. Two different designs are introduced, including tapering the adherend and adhesive fillet. The results show that the inner and outer taper of the adherend has almost no effect on the stress concentration, while a 45° fillet of the adhesive can reduce stress concentration by 50 %. Hildebrand [13] used non-linear analysis to study the effect of fifteen different shapes of the adhesive layer (e.g. tapering, rounding, or denting) at the adhesive-free edges on the strength of metal-Fibre-reinforced plastics (FRP) single lap joints (SLJs). The experimental result is only available for one design (45° adhesive fillet). However, no information is provided to explain the manufacturing procedure and the accuracy of the manufactured sample. The numerical simulation results suggest that a careful adhesive free-end design could improve joint strength by 90–150 percent. Lang and Mallick [14] conducted a comparative finite element (FE) analysis of the different spew fillet designs (square, half triangle, full triangle, half rounded, full rounded, fully rounded with fillet, oval and arc) with a detailed analysis of the adhesive thickness and brief analysis of the spew fillet angles. The results show that the arc design has the best performance, followed by the full rounded with fillet, both with lower peak shear and peel stress values than the other joints. Belingardi et al. [15] conducted detailed studies on various spew fillet angles (75°, 60°, 45°, 30° and 15°). Their results show that the secondary peak stress is higher than the primary peak for a large spew fillet angle. However, this can be avoided for an angle below 45°. Hua et al. [16] studied the effect of using a recess in bond-line with and without spew fillet on composite-titanium single-lap joints. The numerical results show that joint strength almost remained unchanged for joints with a recess length less than 50 %, while a 50 % gap in the overlap length with spew fillet can significantly reduce stress concentration. The majority of the research in the literature focused on stress concentration, and few authors tried to predict full crack path using available FE models such as cohesive zone modelling (CZM) or eXtended finite element model (XFEM) due to convergence problems. The FE model is based on continuum mechanics and produces results by solving the global stiffness equation. The convergence problem mostly arises from the cohesive model's softening effect and negative eigenvalues in the stiffness matrix resulting in inadequate FE equations and an unstable numerical solution [14]. In contrast, the discrete element (DE) is a discontinuous model in which each particle element and interaction is independently recorded and dynamically updated. As a result, the DE model can more efficiently deal with the local material behaviour by creating local parameters for the given particles and contacts [17].

Although many researchers have tried to introduce a new design (Fillet or Recess) to improve stress distribution along the bond-line for adhesively bonded joints, most of these works have been conducted through FE analysis. To the authors' best knowledge, only a few experimental works have been conducted to verify the benefit of these designs. Even though many of these methods have fairly simple designs in the studies, including adding fillet or chamfer at the end of the bond line, it is extremely challenging in practice to manufacture these new designs accurately without using robotic arms due to the nature of the adhesives. However, in this paper, the design flexibility of additive manufacturing (also commonly referred to as 3D printing) enables the production of a sacrificial 3D fixture to produce modified adhesively bonded joints. One of the materials that show promising properties is Polyvinyl Alcohol (PVA), a water-soluble filament normally utilised for support structures. PVA is widely used in medical equipment as well as in many industrial applications [18]. Mohanty et al. [19] used additive manufacturing with sacrificial PVA material to generate structured pores with a high level of control over the interior architecture, which can be tailored to the application's needs. Moreover, pharmaceutical researchers attempted to use fused deposition modelling (FDM) based additive manufacturing and PVA material to fabricate drug delivery systems [20–22]. However, the PVA material is not utilised in manufacturing bonded structures to our best knowledge.

The primary objectives of this work are to manufacture geometrically modified dissimilar bonded joints using additive manufacturing and assess the benefit of these designs using both experimental and numerical data. In order to do this, three different designs are selected from the literature [14–16] based on the stress distribution results. Hybrid joints are produced using two different types of adherends (Aluminium and polyphthalamide (PPA)) and adhesives (Loctite EA 9497 and Araldite 2015). The FE model was used to obtain stress analysis along the bond line, and the DE model was utilised to predict failure load and failure mode in the adhesive bond line.

2. Experiment

2.1. Material selection

Two adherends and adhesives materials were used in this work, with the material properties shown in Table 1. The adhesives are Loctite EA 9497, a brittle epoxy adhesive, and Araldite 2015, a moderately ductile epoxy adhesive. PPA is commercially known as Grivory HTV-5H1 black 9205 and is composed of 50 % glass fibre-reinforced engineering thermoplastic material built on a semi-crystalline, slightly aromatic polyamide. The material properties are obtained [23] through tensile tests based on the ISO EN 485–2:2004 standard for adherends and ISO 527–2 for adhesive.

Polyvinyl Alcohol (PVA (RS-UK)) is a water-soluble thermoplastic that is used as a support structure material for additive manufacturing. Water and chemicals such as glycols (hot), glycerol (hot), piperazine, methylenediamine, formamide, dimethyl sulfoxide, and tetrahydrofuran are recommended solvents for PVA [25]. Since PVA is highly sensitive to moisture, the filament must be stored in a dry environment; otherwise, the absorbed moisture softens the filament and causes air bubbles and cracks during deposition. The literature on using PVA as a support material is extremely limited and unclear [26]. Therefore, several print trials are carried out in order to determine the best parameters for RS-Pro PVA filament used with a Flashforge Finder machine.

2.2. Joint configuration, fabrication and testing

In this work, four types of single-lap joints were fabricated with two different types of adhesives: the unmodified configuration of Single lap joint (SLJ) (without fillet); and the ones with various fillet and recess designs in the adhesive bond-line (shown in Fig. 1). The conventional SLJ (Model-0) is used as a benchmark design. All SLJs are manufactured with the same value of grip-grip separation points ($L_t = 125\,mm$), the thickness of the adherend ($t_s = 3\,mm$), The thickness of the adhesive ($t_A = 1\,mm$), the width of the adherend ($w = 25\,mm$) and the overlap length of the bonding ($L_{AD} = 25\,mm$). At the ends of the joints, $t_{tab} = 25\,mm$ mm tabs are bonded to ensure proper alignment in the testing machine.

The manufacturing process starts by fabricating the fixtures (Fig. 2 a) using PVA filament and print settings (shown in Table 2). The CAD models of the fixture are imported into Simplify3D to generate a g-code for the printer. The major problem with processing PVA is the tendency to absorb moisture from the air, resulting in softening. Therefore, the filament is dried at 55 °C for 8 h using the filament dryer (eSun) before use. The drying process continued during fabrication due to the fact that the filament could absorb enough moisture after 60 min without using the dryer to cause filament feeding problems. The fixtures should be fabricated no more than 24 h before manufacturing the samples as the parts could absorb moisture in the air, resulting in a weakened fixture and a reduced accuracy of the manufactured modified bonded joint. All types of SLJs received the same surface treatment to improve bonding strength. To remove grease spots, the bonding surface is sanded using 60-grit sandpaper and cleaned with compressed air and Acetone (Fig. 2 b). The bond line and the fixture location are marked on the adherend (Fig. 2 b). In order to control adhesive thickness at 1 mm, small wire

Table 1
The bulk property of adherends and adhesives [23,24].

Property	Aluminium (AL) 6082 T6 [23]	Polyphthalamide (PPA) [23]	Loctite EA 9497 [23]	Araldite 2015 [24]	Polyvinyl Alcohol (PVA)
Young Modulus (MPa)	70770 ± 38 0	17620 ± 6 00	7705.35 ± 468.08	1850 ± 210	3860[a]
Yield Stress (MPa)	254.59 ± 3.20	241.33 ± 10.4	46.29 ± 3.13	12.63 ± 0.61	78[a]
Elongation at fracture (%)	10.83 ± 0.95	1.71 ± 0.04	0.71 ± 0.09	4.77 ± 0.15	–
Poisson Ratio	0.30 ± 0.01	0.32 ± 0.04	0.29[a]	0.33[a]	–
Density (tonne/mˆ3)	2.7[a]	1.65[a]	1.1[a]	1.4[a]	0.75[a]

[a] Manufacturer data.

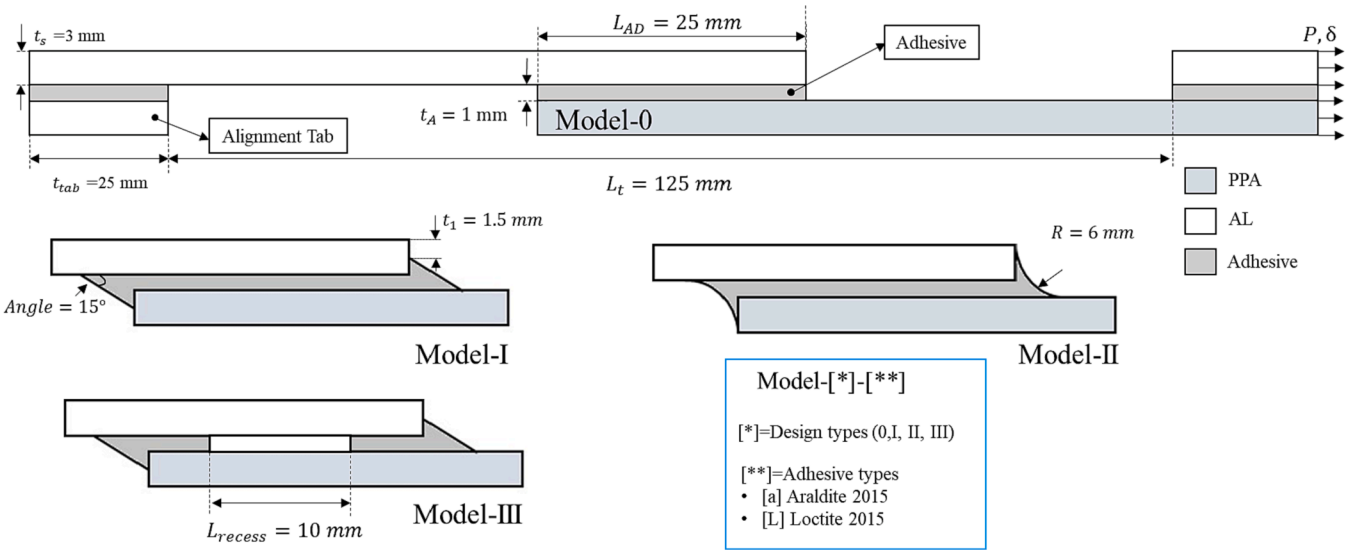

Fig. 1. Dimensions and geometry of SLJs (a) unmodified (without fillet) (b) with fillet and recess.

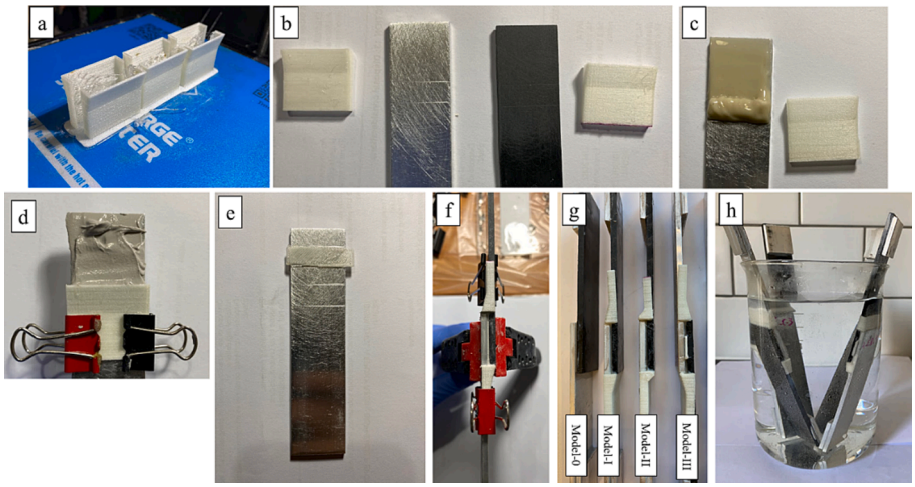

Fig. 2. The process of manufacturing the geometrically modified adhesive-bonded joint: (a) printing PVA fixture (b) cleaning samples (c) applying adhesive (d-e) placing PVA fixture depending on the joint design (f-g) curing adhesive (h) dissolving PVA fixture.

Table 2
Print setting for PVA.

Property	Polyvinyl Alcohol
Layer height (mm)	0.2
Object infill (%)	100
Feedrate (mm/s)	50
Travel feedrate (mm/s)	70
Print temperature (°C)	215

spacers with a diameter of 1 mm are used in the bond line, and the extra adhesive is applied at the end of the bond line to ensure the even spread of the adhesive underneath the fixture (Fig. 2 c-d). An additional step is carried out for the joint with recess by bonding a PVA spacer with a thickness of 1 mm using Cyanoacrylate glue before applying adhesives (Fig. 2 e). The specimens are left at room temperature for seven days to reach the fully cured strength recommended by the manufacturer (Fig. 2 f-g). The PVA fixture is softened during the adhesive curing process (Fig. 2 g). Therefore, most of the fixtures can be removed easily using a flush cutter. However, the samples are left in a beaker full of warm water

for three hours to dissolve the remaining PVA fixture bonded to the adhesive (Fig. 2 h). Duran et al. [26] studied the rate of solubility of PVA in water to find the optimal temperature for water. They recommended using water with a slightly lower temperature than boiling with a high stir rate (at least 1,000 rpm) for around 75 min or more. However, in this work, only a small amount of PVA fixture needs to be dissolved to simplify the manufacturing process; warm water is used for the dissolving procedure. The final samples show high accuracy in terms of the fillet dimensions (Fig. 3).

The tensile tests were carried out with Instron 3380 series machine with a 100 kN load cell at room temperature under displacement control of 0.5 mm/min. The non-contact optical method (Imetrum system) was used to measure displacement and observe the failure process in joints.

2.3. Finite element and discrete element modelling

FEM facilitates the modelling of complicated geometrical and irregular shapes. Thus, three-dimensional models for SLJs with the four different joint configurations were built in Abaqus® (Fig. 4), which provided the stress distributions along the bond line. Adherends and adhesive are meshed by a 4-node linear brick (C3D4R in ABAQUS) with 12 elements in the thickness direction. Even though the FE model can predict failure load in the adhesive using CZM or XFEM, they are not always suitable for capturing the propagation of cracks inside the adhesive. The XFEM model does not require an initial crack or defined crack patch compared to the CZM model, but the convergence issue is the main barrier to using the techniques when the crack starts at the middle of the adhesive and progresses toward the adherend's interface. Although some works tried to combine the XFEM method and surface CZM technique in Abaqus to simulate this type of failure, they all used pre-cracked in the adhesive mainly to overcome convergence issues [27], which limits the capability of these methods. Therefore, the particle-based DE model is adopted in this study to simulate the free initiation and propagation of micro-cracks inside the adhesive and along the interface, which cannot be well simulated by a cohesive FE model.

Trials of DE simulation show that a 2D DE model is adequate to locate the failure process and is thus used to reduce the computational cost. The software package PFC2D is used to generate the tested SLJs. The adherend uses the hexagonal packing to generate a regular pattern of AL and PPA particles within the area, excluding the lap area. The lap area adopts the expansive particle method to generate smaller particles and better contact assignments to the adhesive particles. The contact model between adherend particles adopts the soft bond model, which is able to simulate the ductile and softening behaviour of materials. The theoretical solutions to determine the elastic property of materials using hexagonal packing can be found in [17], which gives the equations for contact stiffness as:

$$\text{Normal contact stiffness} \quad k_n = \frac{2E\lambda}{2\sqrt{3}(1+\nu)}\left(1+\frac{2}{3(1-\nu)}\right) \tag{1}$$

$$\text{Tangential contact stiffness} \quad k_s = \frac{2|(3\nu-1)|E\lambda}{6\sqrt{3}(1-\nu^2)} \tag{2}$$

Where E is the elastic modulus, ν is the Poisson's ratio and λ denotes the particle thickness. The softening factor is 200 for AL and 100 for PPA, with a softening tensile strength factor of 0.9. The calibrated soft bond parameters for the adherend within the lap area are given in Table 3.

The expansive particle packing method is also adapted to generate a randomly dense packing of adhesive particles. The average particle radius of adhesive is set to be half of that used for adherend to guarantee enough contact between adherend and adhesive particles. The soft bond model is also used to flexibly describe the nonlinearity and large strain behaviour of different adhesives. The calibration of microscale contact parameters for adhesives is conducted following the concept that: 1) the elastic modulus should first be calibrated; 2) the Mode I and Mode II fracture energies of thin adhesive-bonded by adherends are subsequently calibrated on the basis of fixing the contact parameters controlling the elastic modulus [28,29]. The calibrated fracture energies of the adhesives are given in Table 4.

It is worth noting that the fracture energies of AL-AL adhesion are obtained via the cohesive fractures of adhesives, as the experimental observation shows that both adhesive types have a cohesive failure when bonding with AL adherends. Thus, the contacts at AL-adhesive interfaces are assumed to be unbreakable. As for the PPA-PPA adhesion, the fracture energies are extracted from the adhesive failure of the PPA-adhesive interface. The PPA-adhesive interface is described with the parallel bond model, which omits the softening stage of bonds. This implies that the interfacial failure occurs simultaneously once the adhesion strength between PPA and adhesive is reached. The calibrated parameters of adhesives are given in Table 5. The bond parameters of the PPA-adhesive interface are shown in Table 6.

The lap area of Model-I SLJ is selected to show the configuration of the DE model, as shown in Fig. 5. As the adherend materials are expected not to achieve their yield (or failure in brittle PPA) strength, the fractures are hence likely to propagate within adhesive particles or PPA-adhesive interface.

3. Results and discussion

3.1. Joint strength

The average failure load is obtained from four tests for each joint. Model-0 is used as a benchmark for comparison purposes. As it is clear from Fig. 6, a modified design generally improves the failure load of the single lap joint. The best performance is achieved with model-II (Curved fillet) with 59.33 % and 43.50 % improvement in failure load for Araldite2015 and Loctite EA9497 adhesives, respectively. Model-I (Triangle fillet) achieved the second-best performance with a 24.97 % improvement for Loctite EA9497 adhesive and 44.75 % for Araldite 2015

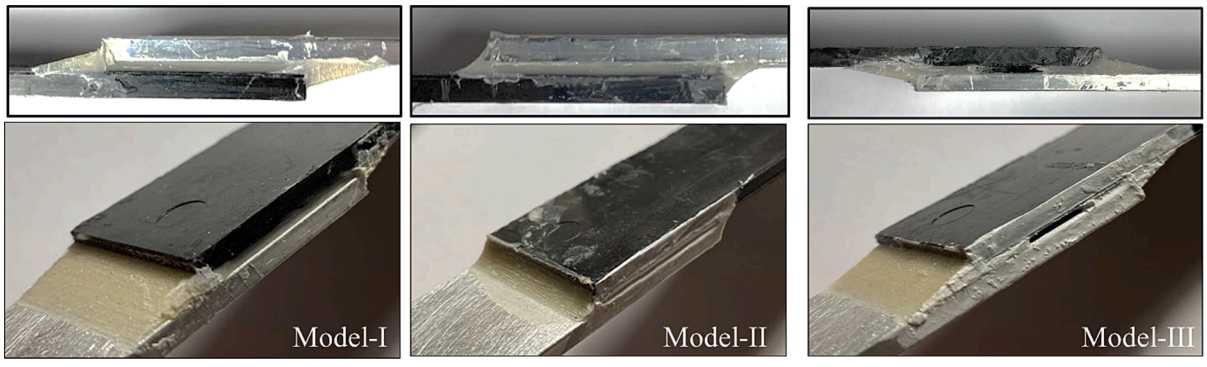

Fig. 3. The final manufactured joints using AM assisted method.

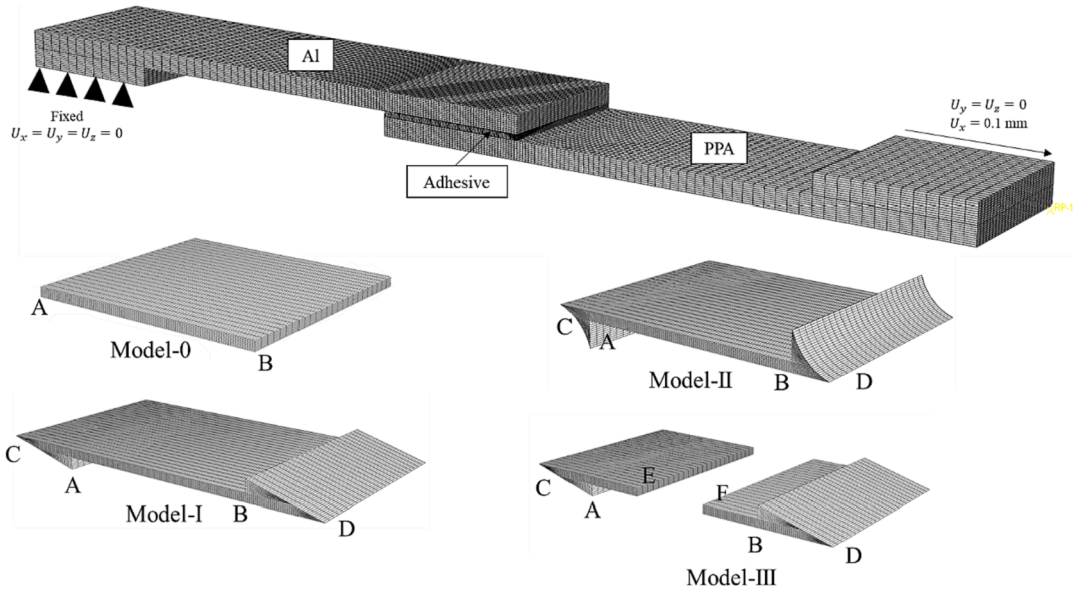

Fig. 4. The FEM models' configurations of modified hybrid adhesively bonded joints.

Table 3
Soft bond parameters for adherend with expansive packing.

Keyword	Description	Value (AL)	Value (PPA)
sb_emod	Effective modulus (MPa)	4.55×10^4	7.87×10^3
sb_kratio	Normal to shear stiffness ratio	3.6	3.6
sb_rmul	Radius multiplier	1.44	1.897
sb_ref_str *	Reference strength of the soft bond (MPa)	280	216
beta*	The ratio of tensile to cohesion strength	0.25	0.25

* user-defined keywords. sb_ref_str is defined as twice the tensile strength of the bond.

Table 4
Calibrated fracture energies of tested adhesives [23,24,30].

Property	Loctite EA 9497 [23] (AL-AL)	(PPA-PPA)	Araldite 2015 (AL-AL) [30]	(PPA-PPA) [24]
G_{IC} (N/mm)	0.26 ± 0.06	0.22 ± 0.04	0.533 ± 0.123	0.43 ± 0.02
G_{IIC} (N/mm)	0.90 ± 0.388	0.46 ± 0.09	3.123 ± 0.203	4.70 ± 0.34

Table 5
Microscale bond parameters of adhesives.

Keyword	Description	Loctite EA 9497	Araldite 2015
sb_emod	Effective modulus (MPa)	3.65×10^3	1.85×10^3
sb_kratio	Normal to shear stiffness ratio	4.7	5.0
sb_rmul	Radius multiplier	1.9	1.0
sb_ref_str*	Reference strength of the soft bond (MPa)	14.0	25.3
beta*	The ratio of tensile to cohesion strength	1.0	0.25

adhesive. The better performance of modified designs in the Araldite 2015 adhesive in comparison to the Loctite EA 9497 can be justified by the lower secondary peak stress at the fillet area (Fig. 10 a and Fig. 11 a). Model-III offers the least improvement with a 5.46 % and 11.93 % increase in failure load of the Loctite EA 9497 and Araldite 2015 adhesives, respectively. The existence of the slot encourages the formation of a through crack along the overlap, which results in a relatively lower overall strength compared with Models I and II. The lower performance

Table 6
Microscale bond parameters of interfaces between adhesive and PPA adherend.

Keyword	Description	Loctite EA 9497	Araldite 2015
pb_kn	Normal stiffness (N/mm^3)	1.0×10^6	6.15×10^5
pb_ks	Shear stiffness (N/mm^3)	2.2×10^5	6.5×10^5
pb_ten	Tensile strength (MPa)	14	23.0
pb_coh	Cohesion (MPa)	8	22.8
pb_fa	Friction angle ()	14	14

of Model-III for Loctite adhesive can be attributed to the brittle nature of this adhesive which makes it sensitive to the extra peak stresses in the middle of the bond line due to the existence of the slot. There is a good agreement between the DEM model and the experimental results for both adhesives (Fig. 7). More accurate failure load estimations were obtained for Loctite adhesives since the interface properties of this adhesive were obtained for PPA adherend in a previous study [23]. For the load–displacement curves of Araldite 2015 samples, it should be noted that the given properties and calibrated data only select the mean value from the literature [24,30], as accurate in-house data from tests on this adhesive were not available, which could be the reason for the deviations from our experiment.

The experimental failure analysis shows that the final failure always occurs at the PPA-adhesive interface in dissimilar SLJs, regardless of the joint configurations. The crack in the bonded joints with ductile adhesive (Araldite 2015) grows gradually from the high-stress points at the end of the bond line (Fig. 8 (b-c)). In contrast, the crack in the epoxy adhesive occurs fast, resulting in the sudden failure of the bond line (Fig. 9 (b)). The failure modes can be captured with DE simulation as the fracture growth within adhesive particles or along the interface can be well traced via bond failure. The failure modes of SLJs are shown in Fig. 8 (a) and 9 (a). Red footprints represent the bond's failures.

3.2. Stress analysis

Fig. 10 represents the comparison of the normalised shear (τ_{xy}/τ_{avg}) and peel (σ_y/τ_{avg}) stress distributions for various joint designs with Loctite EA9497. The adhesive bond line is divided into three sections which contain primary peak stresses (A and B) in the main section of the bond line ($L_0 = 25$ mm) and secondary peak stresses (C and D) in the fillet sections. It is clear that all modified SLJs experience a significant improvement in the primary peak stresses at the end of the bond line (A

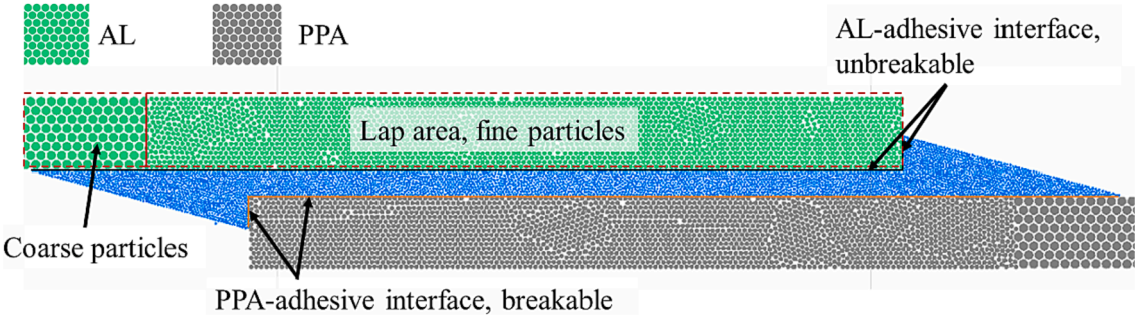

Fig. 5. Lap area in DE model (Model-I SLJ as an example).

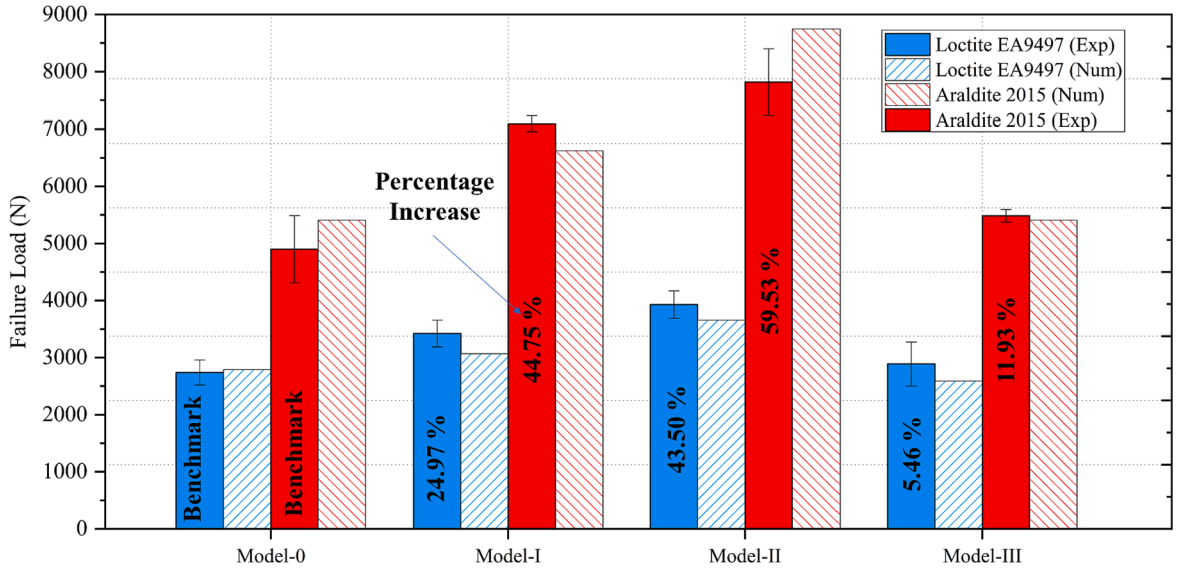

Fig. 6. Comparison of experimental and numerical failure load for different geometrically modified single-lap designs.

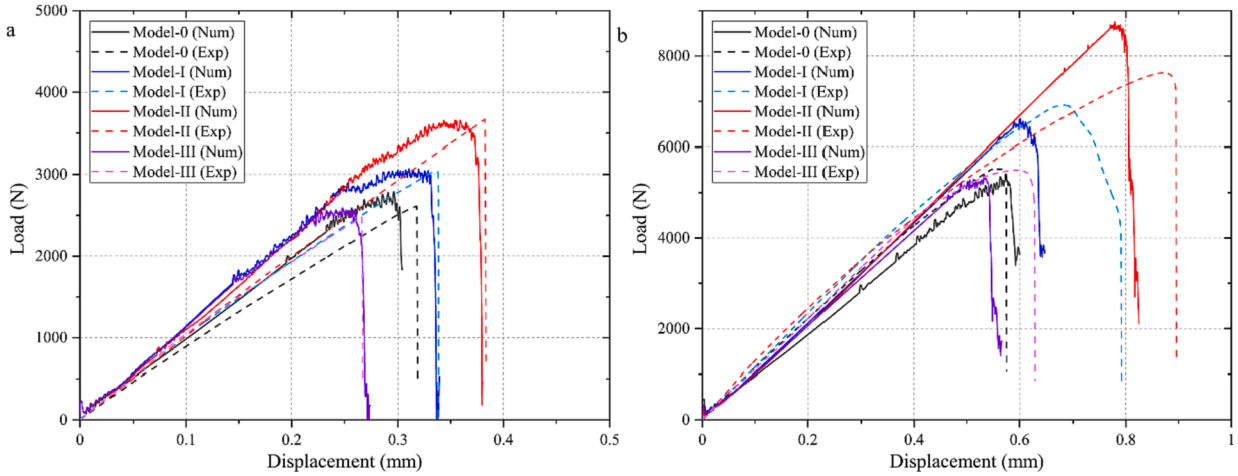

Fig. 7. Load-displacement curve for (a) Loctite EA9497 and (b) Araldite2015.

and B). The maximum primary peak (A and B) values of the τ_{xy}/τ_{avg} decreases from 2.32 in Model-0 to 0.76 in Model-I at section-I (AL side) and 3.87 in Model-0 to 1.55 Model-I at section-III (PPA side), which corresponds to a reduction of 67.24 % and 59.94 %, respectively. In addition, the secondary peak values (C and D) of the τ_{xy}/τ_{avg} in Model-I are still lower than the primary peak stresses (A-B) in model-0 by 53 % and 33 % in section-I and II, respectively. The higher secondary peak (C and D) value in section-II (PPA side) can be justified by the lower stiffness of the PPA. The same trend is observed for the σ_y/τ_{avg}, with 140 % and 83 % reduction of primary peak stresses at section-I and section-III, respectively, when compared with Model-0. The Model-II experiences slightly better improvement of the τ_{xy}/τ_{avg} and σ_y/τ_{avg} at the middle and end of the bond-line. However, the secondary peak stresses in the fillet sections are significantly higher in Model-II compared to Model-I but

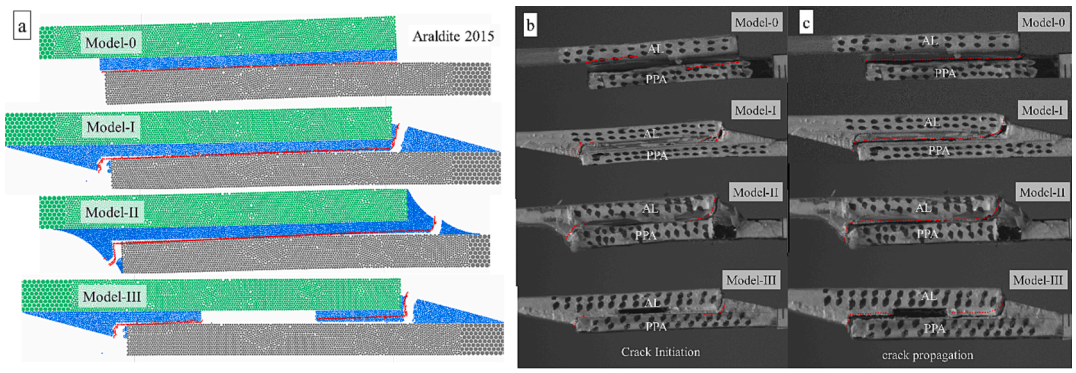

Fig. 8. Numerical and experimental crack and failure type for various SLJs designs of Araldite 2015.

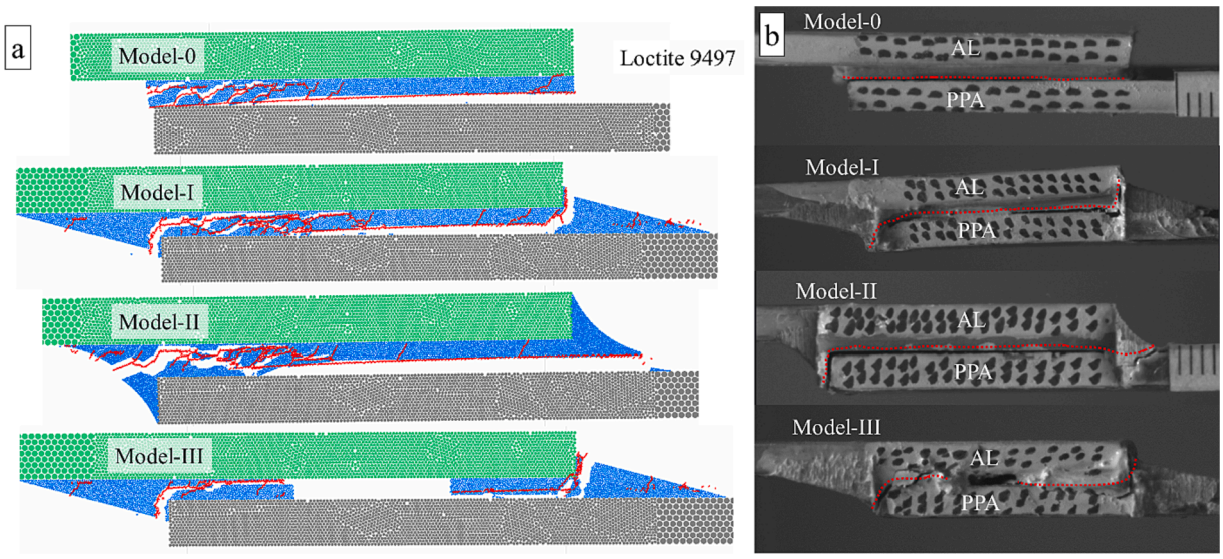

Fig. 9. Numerical and experimental crack and failure type for various SLJs designs of Loctite 9497.

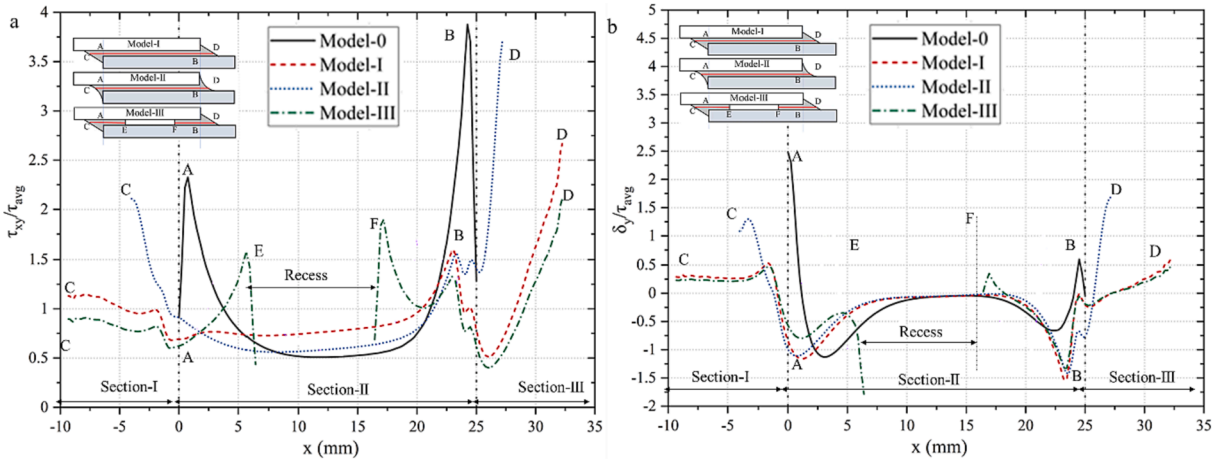

Fig. 10. The comparison of the normalised shear τ_{xy} and peel σ_y stresses at the middle of adhesive for Loctite EA 9497.

lower than the primary peak stresses in Model-0. The lower secondary peak (C and D) in Model-I can be justified by the lower entry angle of the spew fillet [14].

Using a fillet in combination with a recess (Model-III) improves peak shear stress at the end of bond lines by around 20 %. However, extra peak stress is created in the middle of the bond line (E and F), which could adversely affect the joint strength, especially in brittle adhesives, which are sensitive to peak stresses. The recess does not have any effect on the peel stress at the end of the bond line, but it creates extra peak peel stress in the middle of the adhesive (E and F).

It is clear from Fig. 11 that the same τ_{xy}/τ_{avg} stress distribution patterns are observed for the joint with Araldite 2015 adhesive with

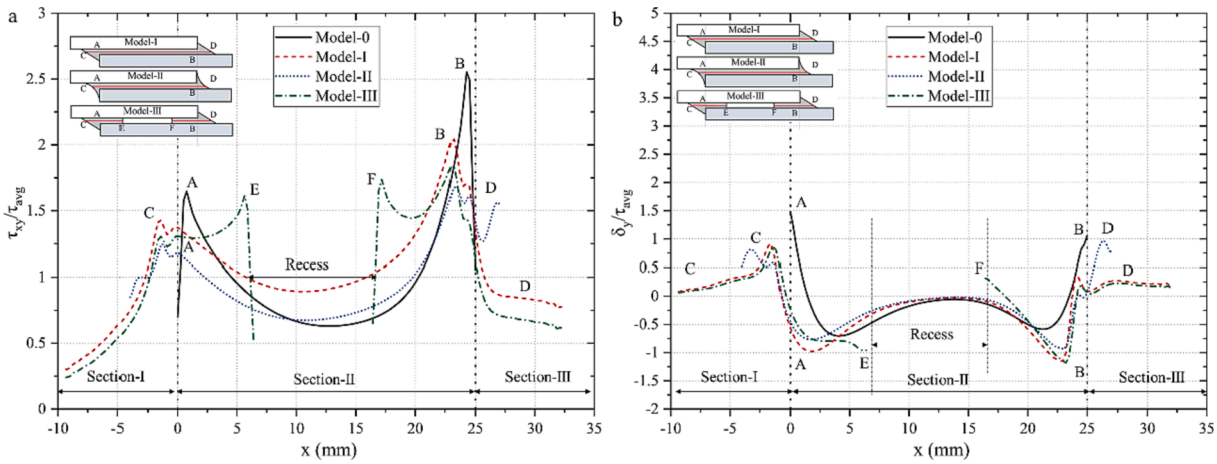

Fig. 11. The comparison of the normalised shear τ_{xy} and peel σ_y stresses at the middle of adhesive for Araldite 2015.

significantly lower secondary peaks (C and D) in the fillet area in comparison to the modified joint with Loctite EA 9497. Conversely, the percentage reduction of the primary peak shear stress is significantly lower for the joint with Araldite 2015 in comparison to the Loctite EA9497. For instance, in Model-I, the peak τ_{xy}/τ_{avg} reduces by 20 % and 17 % on PPA and AL sides, respectively, in comparison to the Model-0. Moreover, it can be seen that Model-II has the lowest primary τ_{xy}/τ_{avg} peak stress on the both sides in comparison to the other modified SLJs. The σ_y/τ_{avg} stress distribution pattern for Araldite 2015 followed the same trend with a minor reduction in secondary peak stress.

4. Conclusion

This work used sacrificial additive manufactured soluble fixtures to produce geometrically modified adhesively bonded joints. The FE models were used to study the stress distribution along the bond line, and the DE models were used to estimate the joint failure load and crack path in the adhesive bond line. The following observations were found from experimental and numerical results:

- Additive manufacturing makes it simple to customise fixtures accurately to any form, which can be used to create the required fillet shape at the end of adhesive bond lines. Following curing of the adhesive, the sacrificial fixture can be dissolved in water. This has minimal effect on the strength of the bond line as the samples are submerged in water for a short period.
- A modified bonded joint may have secondary and primary peak stresses along the bond line, yet these stresses are significantly lower than the peak stresses at the end of a conventional bonded joint. As a result, the geometrically modified bonded joints outperformed the conventional bonded joint regardless of the adhesive types. The failure load in the joint with ductile triangle fillet improved twice as much as the epoxy-one, which can be justified by the lower secondary peak stress at the fillet area in ductile adhesive.
- Regardless of the joint configurations, the final failure occurs at the PPA-adhesive interface in different SLJs. The fracture in the ductile adhesive-bonded joints develops progressively from the high-stress locations at the bond line's end, while the epoxy adhesive failure is sudden. This can be justified brittle adhesives are more sensitive to primary and secondary peak stresses. The failure mechanisms can be reproduced via DE modelling as the fracture progression inside adhesive particles or at the interface could be traced via bond failure between discrete elements.

Data availability

The raw/processed data required to reproduce these findings are available in this paper.

CRediT authorship contribution statement

Armin Yousefi Kanani: Conceptualization, Methodology, Investigation, Software, Writing – original draft. **Xing-Er Wang:** Methodology, Software. **Xiaonan Hou:** Conceptualization, Project administration, Funding acquisition, Writing – review & editing. **Allan E.W. Rennie:** Conceptualization, Writing – review & editing. **Jianqiao Ye:** Writing – review & editing.

Declaration of Competing Interest

The authors declare that they have no known competing financial interests or personal relationships that could have appeared to influence the work reported in this paper.

Data availability

Data will be made available on request.

Acknowledgements

This work is financially supported by the United Kingdom Engineering and Physical Sciences Research Council [Grant No. EP/T020695/1]. All research data supporting this publication are directly available within the publication.

References

[1] Waite C. National Statestic, UK Greenhouse Gas Emissions; 2018. [Online]. Available: https://assets.publishing.service.gov.uk/government/uploads/system/uploads/attachment_data/file/863325/2018-final-emissions-statistics-summary.pdf.
[2] ICCT. European vehicle market statistics; *2017/18*. https://theicct.org/sites/default/files/publications/ICCT_Pocketbook_2017_Web.pdf (accessed May 20, 2020).
[3] Matthews FL, Kilty PF, Godwin EW. A review of the strength of joints in fibre-reinforced plastics. Part 2. Adhesively bonded joints. Composites Jan. 1982;13(1):29–37. https://doi.org/10.1016/0010-4361(82)90168-9.
[4] Shang X, Marques EAS, Machado JJM, Carbas RJC, Jiang D, da Silva LFM. Review on techniques to improve the strength of adhesive joints with composite adherends. Compos Part B Eng Nov. 2019;177:107363. https://doi.org/10.1016/J.COMPOSITESB.2019.107363.
[5] Nemati Giv A, Ayatollahi MR, Ghaffari SH, da Silva LFM. Effect of reinforcements at different scales on mechanical properties of epoxy adhesives and adhesive joints: a review. J Adhes Nov. 2018;94(13):1082–121. https://doi.org/10.1080/00218464.2018.1452736.

[6] Hacısalihoglu İ, Akpinar S. The effect of stepped notches and recesses on joint strength in adhesive bonded joints: Experimental and numerical analysis. Theor Appl Fract Mech 2022;119:103364.
[7] Kanani AY, Hou X, Ye J. The influence of notching and mixed-adhesives at the bonding area on the strength and stress distribution of dissimilar single-lap joints. Compos Struct Jun. 2020;241:112136. https://doi.org/10.1016/j.compstruct.2020.112136.
[8] Akpinar S. The strength of the adhesively bonded step-lap joints for different step numbers. Compos Part B Eng Dec. 2014;67:170–8. https://doi.org/10.1016/j.compositesb.2014.06.023.
[9] Cognard JY, Créac'hcadec R, Maurice J. Numerical analysis of the stress distribution in single-lap shear tests under elastic assumption—Application to the optimisation of the mechanical behaviour. Int J Adhes Adhes 2011;31(7):715–24.
[10] Sawa T, Liu J, Nakano K, Tanaka J. Two-dimensional stress analysis of single-lap adhesive joints of dissimilar adherends subjected to tensile loads. J Adhes Sci Technol 2000;14(1):43–66. https://doi.org/10.1163/156856100742104.
[11] Ribeiro TEA, Campilho RDSG, da Silva LFM, Goglio L. Damage analysis of composite–aluminium adhesively-bonded single-lap joints. Compos Struct Feb. 2016;136:25–33. https://doi.org/10.1016/J.COMPSTRUCT.2015.09.054.
[12] da Silva LFM, Adams RD. Techniques to reduce the peel stresses in adhesive joints with composites. Int J Adhes Adhes Apr. 2007;27(3):227–35. https://doi.org/10.1016/j.ijadhadh.2006.04.001.
[13] Hildebrand M. Non-linear analysis and optimisation of adhesively bonded single lap joints between fibre-reinforced plastics and metals. Int J Adhes Adhes Oct. 1994;14(4):261–7. https://doi.org/10.1016/0143-7496(94)90039-6.
[14] Lang TP, Mallick PK. Effect of spew geometry on stresses in single lap adhesive joints. Int J Adhes Adhes Jun. 1998;18(3):167–77. https://doi.org/10.1016/S0143-7496(97)00056-0.
[15] Belingardi G, Goglio L, Tarditi A. Investigating the effect of spew and chamfer size on the stresses in metal/plastics adhesive joints. Int J Adhes Adhes Jan. 2002;22(4):273–82. https://doi.org/10.1016/S0143-7496(02)00004-0.
[16] Hua Y, Gu L, Trogdon M. Three-dimensional modeling of carbon/epoxy to titanium single-lap joints with variable adhesive recess length. Int J Adhes Adhes Oct. 2012;38:25–30. https://doi.org/10.1016/j.ijadhadh.2012.06.003.
[17] Ismail Y, Sheng Y, Yang D, Ye J. Discrete element modelling of unidirectional fibre-reinforced polymers under transverse tension. Compos Part B Eng 2015;73:118–25. https://doi.org/10.1016/j.compositesb.2014.12.024.
[18] Baker MI, Walsh SP, Schwartz Z, Boyan BD. A review of polyvinyl alcohol and its uses in cartilage and orthopedic applications. J Biomed Mater Res Part B Appl Biomater Jul. 2012;100B(5):1451–7. https://doi.org/10.1002/jbm.b.32694.
[19] Mohanty S, Larsen LB, Trifol J, Szabo P, Burri HVR, Canali C, et al. Fabrication of scalable and structured tissue engineering scaffolds using water dissolvable sacrificial 3D printed moulds. Mater Sci Eng C Oct. 2015;55:569–78. https://doi.org/10.1016/j.msec.2015.06.002.
[20] Goyanes A, Buanz ABM, Hatton GB, Gaisford S, Basit AW. 3D printing of modified-release aminosalicylate (4-ASA and 5-ASA) tablets. Eur J Pharm Biopharm Jan. 2015;89:157–62. https://doi.org/10.1016/j.ejpb.2014.12.003.
[21] Goyanes A, Robles Martinez P, Buanz A, Basit AW, Gaisford S. Effect of geometry on drug release from 3D printed tablets. Int J Pharm Oct. 2015;494(2):657–63. https://doi.org/10.1016/j.ijpharm.2015.04.069.
[22] Alhijjaj M, Belton P, Qi S. An investigation into the use of polymer blends to improve the printability of and regulate drug release from pharmaceutical solid dispersions prepared via fused deposition modeling (FDM) 3D printing. Eur J Pharm Biopharm Nov. 2016;108:111–25. https://doi.org/10.1016/j.ejpb.2016.08.016.
[23] Kanani AY, Liu Y, Hughes DJ, Ye J, Hou X. Fracture mechanisms of hybrid adhesive bonded joints: Effects of the stiffness of constituents. Int J Adhes Adhes Oct. 2020;102:102649. https://doi.org/10.1016/j.ijadhadh.2020.102649.
[24] Campilho RDSG, Banea MD, Neto JABP, da Silva LFM. Modelling adhesive joints with cohesive zone models: effect of the cohesive law shape of the adhesive layer. Int J Adhes Adhes Jul. 2013;44:48–56. https://doi.org/10.1016/j.ijadhadh.2013.02.006.
[25] ASTM International. ASTM D5226–21, Standard Practice for Dissolving Polymer Materials. West Conshohocken; 2021.
[26] Duran C, Subbian V, Giovanetti MT, Simkins JR, Beyette Jr FR. Experimental desktop 3D printing using dual extrusion and water-soluble polyvinyl alcohol. Rapid Prototyp J Aug. 2015;21(5):528–34. https://doi.org/10.1108/RPJ-09-2014-0117.
[27] Stuparu F, Constantinescu DM, Apostol DA, Sandu M. A Combined Cohesive Elements—XFEM Approach for Analyzing Crack Propagation in Bonded Joints. J Adhes 2016;92(7–9):535–52. https://doi.org/10.1080/00218464.2015.1115355.
[28] Wang X-e, Kanani AY, Pang K, Yang J, Ye J, Hou X. A novel genetic expression programming assisted calibration strategy for discrete element models of composite joints with ductile adhesives. Thin-Walled Struct 2022;180:109985.
[29] Wang X, Kanani AY, Gu Z, Yang J, Ye J, Hou X. Estimating microscale DE parameters of brittle adhesive joints using genetic expression programming. Int J Adhes Adhes Oct. 2022;118(March):103230. https://doi.org/10.1016/j.ijadhadh.2022.103230.
[30] Carvalho UTF, Campilho RDSG. International Journal of Adhesion and Adhesives Validation of pure tensile and shear cohesive laws obtained by the direct method with single-lap joints. Int J Adhes Adhes 2017;77(April):41–50. https://doi.org/10.1016/j.ijadhadh.2017.04.002.